

# Marchenko method for monitoring induced seismicity with virtual receivers

Kees Wapenaar, Joeri Brackenhoff and Jan Thorbecke, Delft University of Technology

## SUMMARY

The Marchenko method can be used to retrieve Green’s functions (including multiple scattering) between virtual sources in the subsurface and physical receivers at the surface or virtual receivers in the subsurface. Here we discuss a variant of the Marchenko method which retrieves the response between physical sources and virtual receivers in the subsurface. We discuss the theory and illustrate it with numerical examples. The main application of the proposed method is monitoring of induced seismicity with virtual receivers in the subsurface.

## INTRODUCTION

The Marchenko method was originally introduced as a data-driven way to retrieve the Green’s function between a *virtual source* in the subsurface and *physical receivers* at the surface (Broggini and Snieder, 2012; Wapenaar et al., 2013). The required input consists of reflection data at the surface and an estimate of the direct arrivals between the receivers at the surface and the designated position of the virtual source in the subsurface. The retrieved Green’s function properly accounts for primaries and internal multiples and, optionally, also for surface-related multiples (Singh et al., 2015). The retrieved Green’s functions can be used for obtaining a subsurface image, free of artefacts related to multiple scattering (Wapenaar et al., 2014; Slob et al., 2014; Broggin et al., 2014; Ravasi et al., 2016). Subsequently, the Marchenko method has been extended to create not only *virtual sources* but also *virtual receivers* in the subsurface. In other words, the Green’s functions, including multiple scattering, can be obtained between any two points in the subsurface (Wapenaar et al., 2016, 2018; Singh and Snieder, 2017; Brackenhoff et al., 2018). Also these Green’s functions can be used for obtaining accurate images without contamination by multiples (Staring et al., 2017). Another interesting application is data-driven modelling of responses to induced earthquakes. In this application the virtual sources represent potential future earthquakes and the virtual receivers monitor the waves emitted by these virtually induced earthquakes along their complex paths from the source to the surface.

In the current paper we discuss a method to monitor the wave field of *physical* induced seismic *sources* by *virtual receivers* throughout the subsurface. As input the proposed method requires active reflection data at the surface and passive observations (also at the surface) of the responses to the induced earthquakes in the subsurface. The reflection data (in combination with estimates of direct arrivals) are used to derive focusing functions with the Marchenko method (this is the same as in the methods mentioned above). Subsequently, these focusing functions are applied to the passive responses to create virtual receivers in the subsurface, which register the response to the physical induced earthquakes. A complication in comparison with the methods discussed above is that the induced

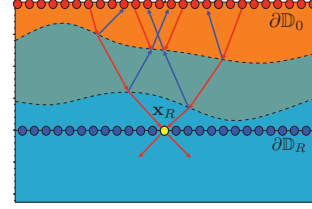


Figure 1: Focusing function  $f_1^+(\mathbf{x}, \mathbf{x}_R, \omega)$  (red rays) and  $f_1^-(\mathbf{x}, \mathbf{x}_R, \omega)$  (blue rays) in a truncated medium.

earthquake sources may be distributed in space and emit unknown non-zero-phase signals at unknown times. Hence, time-symmetry assumptions used in other Marchenko applications do not hold for this application. We discuss the theoretical aspects and analyse the limiting effects of the complexity of the source distribution. We illustrate the method with a numerical example.

## GREEN’S FUNCTION REPRESENTATIONS

Our starting point is the following single-sided Green’s function representation in the frequency domain (Wapenaar et al. (2017), equation (A-26))

$$G(\mathbf{x}_R, \mathbf{x}_S, \omega) + H(z_R - z_S) 2j \Im \{ f_1(\mathbf{x}_S, \mathbf{x}_R, \omega) \} = \int_{\partial \mathbb{D}_0} F(\mathbf{x}, \mathbf{x}_R, \omega) G(\mathbf{x}, \mathbf{x}_S, \omega) d\mathbf{x}, \quad (1)$$

with

$$f_1(\mathbf{x}, \mathbf{x}_R, \omega) = f_1^+(\mathbf{x}, \mathbf{x}_R, \omega) + f_1^-(\mathbf{x}, \mathbf{x}_R, \omega), \quad (2)$$

$$F(\mathbf{x}, \mathbf{x}_R, \omega) = -\frac{2}{j\omega\rho(\mathbf{x})} \partial_3 (f_1^+(\mathbf{x}, \mathbf{x}_R, \omega) - \{f_1^-(\mathbf{x}, \mathbf{x}_R, \omega)\}^*). \quad (3)$$

In equation (1), the Green’s function  $G(\mathbf{x}, \mathbf{x}_S, \omega)$  under the integral may be seen as the passive response to an idealised physical point source at  $\mathbf{x}_S$  in the subsurface, observed by a receiver at  $\mathbf{x}$  at the surface  $\partial \mathbb{D}_0$ . The focusing function  $F(\mathbf{x}, \mathbf{x}_R, \omega)$ , consisting of down- and upgoing parts as specified in equation (3) and illustrated in Figure 1, is retrieved by the Marchenko method from reflection data at the surface (for this we refer to the papers mentioned in the introduction). The Green’s function  $G(\mathbf{x}_R, \mathbf{x}_S, \omega)$  on the left-hand side of equation (1) is the response between the physical source at  $\mathbf{x}_S$  and any virtual receiver at  $\mathbf{x}_R$  in the subsurface. This is the desired response, but unfortunately it is distorted by the other term on the left-hand side of equation (1), in which  $\Im$  denotes the imaginary part,  $j$  is the imaginary unit, and  $H(z)$  denotes the Heaviside function. Finally,  $\rho$  in equation (3) is the mass density and the superscript asterisk denotes complex conjugation.

In the next section we extend equation (1) to account for more realistic sources. Here we illustrate this equation and a vari-

## Monitoring induced seismicity

ant with numerical examples. We obtain this variant by interchanging  $\mathbf{x}_R$  with  $\mathbf{x}_S$  and applying reciprocity to the Green's functions:

$$\begin{aligned} G(\mathbf{x}_R, \mathbf{x}_S, \omega) + H(z_S - z_R) 2j\mathfrak{I}\{f_1(\mathbf{x}_R, \mathbf{x}_S, \omega)\} \\ = \int_{\partial\mathbb{D}_0} G(\mathbf{x}_R, \mathbf{x}, \omega) F(\mathbf{x}, \mathbf{x}_S, \omega) d\mathbf{x}. \end{aligned} \quad (4)$$

For our example, we reformulate equations (1) and (4) for the 1D situation in the time domain, according to

$$\begin{aligned} G(z_R, z_S, t) + H(z_R - z_S)\{f_1(z_S, z_R, t) - f_1(z_S, z_R, -t)\} \\ = F(z_0, z_R, t) * G(z_0, z_S, t), \end{aligned} \quad (5)$$

$$\begin{aligned} G(z_R, z_S, t) + H(z_S - z_R)\{f_1(z_R, z_S, t) - f_1(z_R, z_S, -t)\} \\ = G(z_R, z_0, t) * F(z_0, z_S, t), \end{aligned} \quad (6)$$

where the inline asterisk denotes temporal convolution and  $z_0$  denotes the depth level of  $\partial\mathbb{D}_0$ . We illustrate both expressions for the horizontally layered medium shown in Figure 2(a). The blue dashed line at  $z = 3600$  m denotes the depth of the idealised physical source. Figure 2(b) is the 1D Green's function  $G(z_0, z, t) = G(z, z_0, t)$  for fixed  $z_0 = 0$  and variable  $z$ . Figure 2(c) is the 1D focusing function  $F(z_0, z, t)$ , for  $z_0 = 0$  and variable focus depth  $z$ .

First we evaluate the right-hand side of equation (5) for a fixed physical source depth  $z_S = 3600$  m and variable virtual receiver depth  $z_R$ . To this end we convolve the trace at  $z = z_S = 3600$  m in Figure 2(b) (denoted by the blue dashed line) with all traces in Figure 2(c). The result is shown in Figure 3(a). According to the left-hand side of equation (5), this gives the Green's function  $G(z_R, z_S, t)$  as long as  $z_R < z_S$ . Hence, above the blue dashed line at  $z_R = z_S = 3600$  m, Figure 3(a) represents the Green's function  $G(z_R, z_S, t)$ . Below the blue dashed line the Green's function is distorted by the second term on the left-hand side of equation (5). This term vanishes right of the red dashed line in Figure 3(a), i.e., beyond the direct arrival.

Next we evaluate the right-hand side of equation (6), again for fixed  $z_S = 3600$  m and variable  $z_R$ . To this end we convolve the trace at  $z = z_S = 3600$  m in Figure 2(c) (denoted by the blue dashed line) with all traces in Figure 2(b). The result is shown in Figure 3(b). According to the left-hand side of equation (6), this gives the Green's function  $G(z_R, z_S, t)$  as long as  $z_R > z_S$ . Hence, below the blue dashed line at  $z_R = z_S = 3600$  m, Figure 3(b) represents the Green's function  $G(z_R, z_S, t)$ . Above the blue dashed line the Green's function is distorted by the second term on the left-hand side of equation (6). This term vanishes right of the red dashed line in Figure 3(b), i.e., beyond the direct arrival.

There are three ways to obtain the undistorted Green's function  $G(z_R, z_S, t)$ : (i) summing equation (5) and its time-reversal; (ii) summing equation (6) and its time-reversal; (iii) combining equation (5) for  $z_R < z_S$  with equation (6) for  $z_R > z_S$ , see Figure 3(c) for an illustration. Similar methods hold for the 3D equations (1) and (4). Methods (i) and (ii) yield the so-called homogeneous Green's function (Wapenaar et al., 2016), whereas method (iii) yields the causal Green's function (Singh and Snieder, 2017). All three methods break down when the Green's functions are convolved with an unknown distribution of non-zero-phase source signals.

## INDUCED SEISMICITY REPRESENTATIONS

Let  $s(\mathbf{x}_S, \omega)$  represent the Fourier transform of a distribution of induced seismic sources, confined to some finite source domain  $\mathbb{D}_S$ . We define its response  $u(\mathbf{x}, \omega)$  as

$$u(\mathbf{x}, \omega) = \int_{\mathbb{D}_S} G(\mathbf{x}, \mathbf{x}_S, \omega) s(\mathbf{x}_S, \omega) d\mathbf{x}_S. \quad (7)$$

Applying the operation  $\int_{\mathbb{D}_S} \{\cdot\} s(\mathbf{x}_S, \omega) d\mathbf{x}_S$  to both sides of equation (1) and interchanging the order of integrations on the right-hand side gives

$$\begin{aligned} u(\mathbf{x}_R, \omega) + \int_{\mathbb{D}_S} H(z_R - z_S) 2j\mathfrak{I}\{f_1(\mathbf{x}_S, \mathbf{x}_R, \omega)\} s(\mathbf{x}_S, \omega) d\mathbf{x}_S \\ = \int_{\partial\mathbb{D}_0} F(\mathbf{x}, \mathbf{x}_R, \omega) u(\mathbf{x}, \omega) d\mathbf{x}. \end{aligned} \quad (8)$$

Here  $u(\mathbf{x}, \omega)$  on the right-hand side is the passive response to the physical source distribution, observed by physical receivers at the surface  $\partial\mathbb{D}_0$ , whereas  $u(\mathbf{x}_R, \omega)$  on the left-hand side is the same response, but observed by virtual receivers in the subsurface. Van der Neut et al. (2017) derived an expression like this as the basis for photoacoustic imaging. They assume that  $s(\mathbf{x}_S, \omega)$  is zero phase, which is a reasonable assumption for photoacoustic experiments, in which all sources go off simultaneously. Hence, by taking the real part of both sides of equation (8), the integral on the left-hand side vanishes.

Here we use equation (8) as the basis for monitoring induced seismicity by virtual receivers in the subsurface. For this application  $s(\mathbf{x}_S, \omega)$  is in general not zero phase (think of a rupture process along a fault plane (Kwiatek, 2008)), hence, the integral on the left-hand side will not vanish by taking the real part. Moreover, since the source function is unknown, this integral is unknown as well. Note, however, that due to the Heaviside function, this integral vanishes for all  $\mathbf{x}_R$  above the shallowest source (comparable with the 1D example in Figure 3(a), which shows the correct Green's function above the blue dashed line). Hence, for virtual receivers above the shallowest source, equation (8) simplifies to (rewritten in the time domain)

$$u(\mathbf{x}_R, t) = \int_{\partial\mathbb{D}_0} F(\mathbf{x}, \mathbf{x}_R, t) * u(\mathbf{x}, t) d\mathbf{x}, \quad z_R < z_{S, \min}. \quad (9)$$

This expression replaces the intuitive microseismic imaging condition of Behura and Snieder (2013), which contains the time-reversed Marchenko-retrieved Green's function instead of the focusing function  $F(\mathbf{x}, \mathbf{x}_R, t)$ .

We illustrate equation (9) with a numerical example. Figure 4(a) shows a horizontally layered medium with a constant velocity of 1800 m/s and mass densities of 1500, 2000 and 2500 kg/m<sup>3</sup>. The red line in the deepest layer represents a rupturing fault plane. The rupture starts at the lower left point, propagates with a velocity of 471 m/s along the fault, and ends at the upper right point. We simulate this by letting 100 point sources go off along the fault plane (from lower left to upper right), with 6 ms time intervals. The sources emit signals with a center frequency of 25 Hz, with random peak amplitudes (if the amplitudes were the same, the "moving source" would only emit evanescent waves because the phase slowness along the fault plane is higher than the wave propagation slowness).

## Monitoring induced seismicity

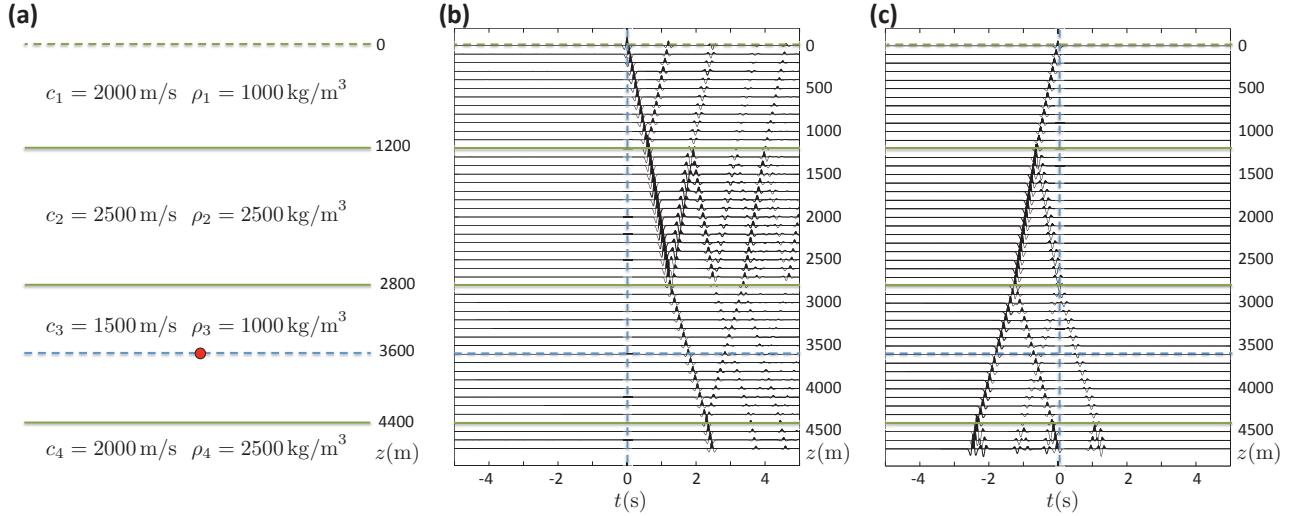


Figure 2: (a) Horizontally layered medium, embedded between two homogeneous half spaces. (b) Green's function  $G(z_0, z, t) = G(z, z_0, t)$  for fixed  $z_0$  and variable  $z$ . (c) Focusing function  $F(z_0, z, t)$  for fixed  $z_0$  and variable focus depth  $z$ .

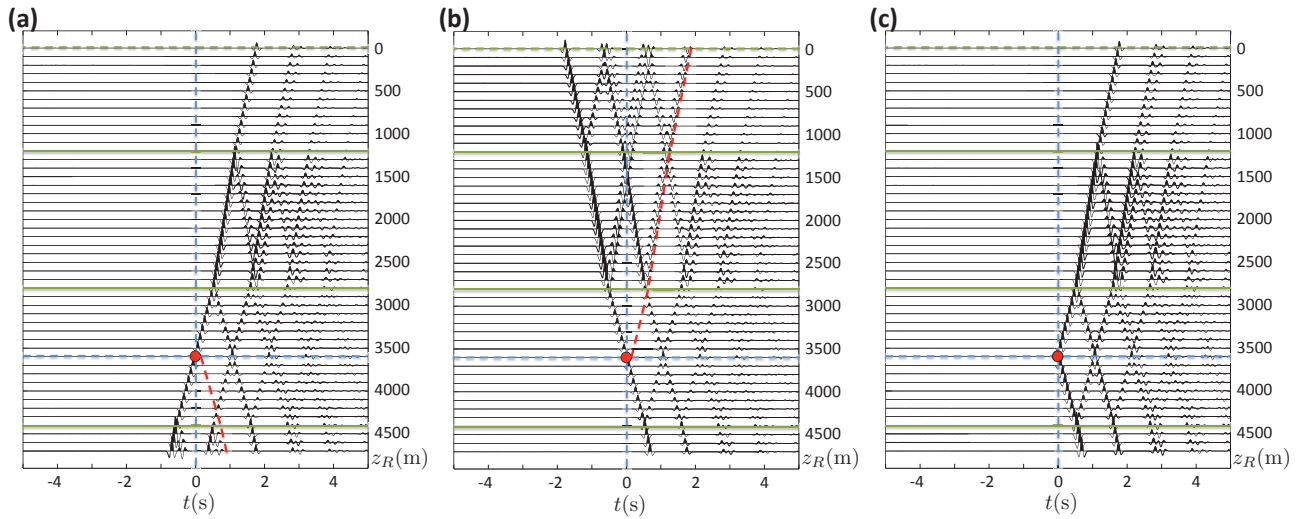


Figure 3: (a) Evaluation of  $F(z_0, z_R, t) * G(z_0, z_S, t)$  for fixed  $z_S = 3600$  m and variable  $z_R$ , hence the blue-dashed trace of Figure 2(b), convolved with all traces of Figure 2(c). (b) Evaluation of  $G(z_R, z_0, t) * F(z_0, z_S, t)$  for fixed  $z_S = 3600$  m and variable  $z_R$ , hence the blue-dashed trace of Figure 2(c), convolved with all traces of Figure 2(b). (c) Green's function  $G(z_R, z_S, t)$ , obtained by combining figure (a) for  $z_R < z_S$  with figure (b) for  $z_R > z_S$ .

## Monitoring induced seismicity

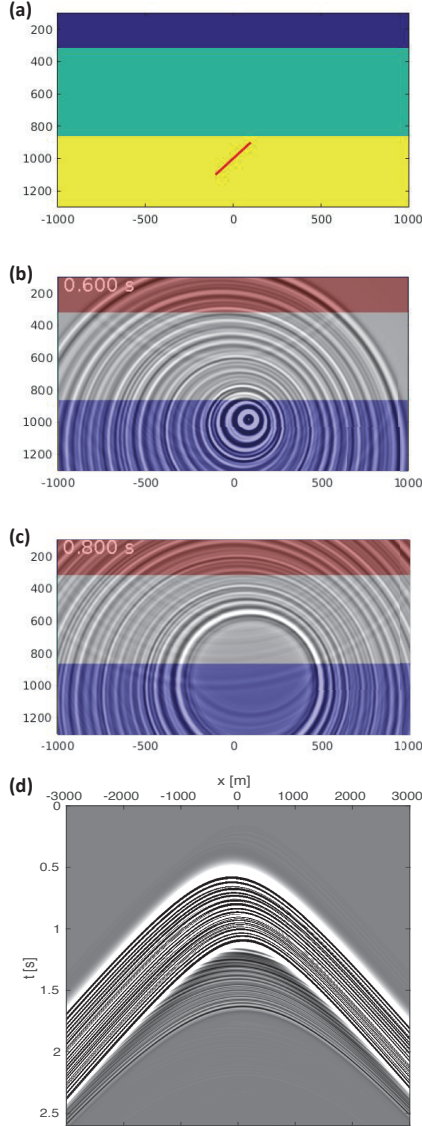


Figure 4: A rupturing fault plane and its seismic response.

Figures 4(b) and 4(c) show snapshots at  $t = 0.6$  s and  $t = 0.8$  s of the complex wave field emitted by the rupturing fault plane. The first snapshot (at  $t = 0.6$  s) is taken at the time that the last source (at the upper right of the fault plane) goes off. The central dark spot in the third layer is the response to this source. The circles around it are responses to deeper sources that went off earlier. The response  $u(\mathbf{x}, t)$ , observed by physical receivers at the surface, is shown in Figure 4(d). This response clearly shows primaries and internal multiples (free-surface multiples are not included, but the proposed method can be extended to account for those as well).

We also model the reflection response of the medium in Figure 4(a) (but without the fault plane) and use this reflection response, together with an estimate of the first arrivals, to retrieve the focusing function  $F(\mathbf{x}, \mathbf{x}_R, t)$  for any virtual receiver position  $\mathbf{x}_R$  in the subsurface.

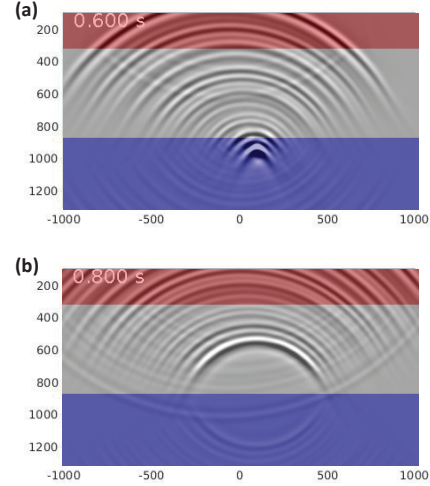


Figure 5: Response to physical induced seismic sources, observed by virtual receivers in the subsurface.

Next we evaluate equation (9) and extract snapshots of  $u(\mathbf{x}_R, t)$  for  $t = 0.6$  s and  $t = 0.8$  s, see Figures 5(a) and (b), respectively. In the first two layers (which are entirely above the shallowest source), these snapshots resemble the directly modeled snapshots in Figure 4 reasonably well. The resolution is somewhat lower, several artefacts are visible, and the (near-) horizontal waves are not recovered. However, direct waves as well as multiples are clearly visible. As expected, the field in the lower layer is not correctly recovered, because the condition  $z_R < z_{S,\min}$  does not hold in that layer.

## CONCLUSIONS

We have discussed a variant of the Marchenko method to create virtual receivers in the subsurface which observe the response to a distribution of unknown physical sources in the subsurface. Similar as in other applications of the Marchenko method, the retrieved response accounts for multiple scattering. Unlike in other applications, the spatial domain in which the method can be applied is limited to the region above the shallowest source (this is because the complex and unknown source distribution prevents taking advantage of time symmetry properties). Despite this limitation, we foresee applications of the proposed method for quantitative characterisation and monitoring of induced seismic sources and their responses. In the numerical example the sources and overburden are relatively simple. The proposed method will become particularly relevant when the sources have complex radiation properties (moment tensors) and when a complex overburden blurs the response to these sources.

## ACKNOWLEDGEMENTS

We acknowledge funding from the European Research Council (ERC) under the European Union's Horizon 2020 research and innovation programme (grant agreement No: 742703).

## Monitoring induced seismicity

### REFERENCES

- Behura, J., and R. Snieder, 2013, Imaging direct- as well as scattered-events in microseismic data using inverse scattering theory: 83rd Annual International Meeting, SEG, Expanded Abstracts, 2019–2023.
- Brackenhoff, J., J. Thorbecke, and K. Wapenaar, 2018, Homogeneous Green's function retrieval on field data using the Marchenko method: 80th Annual International Meeting, EAGE, Extended Abstracts, (accepted).
- Broggini, F., and R. Snieder, 2012, Connection of scattering principles: a visual and mathematical tour: *European Journal of Physics*, **33**, 593–613.
- Broggini, F., R. Snieder, and K. Wapenaar, 2014, Data-driven wavefield focusing and imaging with multidimensional deconvolution: Numerical examples for reflection data with internal multiples: *Geophysics*, **79**, WA107–WA115.
- Kwiatek, G., 2008, Relative source time functions of seismic events at the Rudna copper mine, Poland: estimation of inversion uncertainties: *Journal of Seismology*, **12**, 499–517.
- Ravasi, M., I. Vasconcelos, A. Kritski, A. Curtis, C. A. da Costa Filho, and G. A. Meles, 2016, Target-oriented Marchenko imaging of a North Sea field: *Geophysical Journal International*, **205**, 99–104.
- Singh, S., and R. Snieder, 2017, Source-receiver Marchenko redatuming: Obtaining virtual receivers and virtual sources in the subsurface: *Geophysics*, **82**, Q13–Q21.
- Singh, S., R. Snieder, J. Behura, J. van der Neut, K. Wapenaar, and E. Slob, 2015, Marchenko imaging: Imaging with primaries, internal multiples, and free-surface multiples: *Geophysics*, **80**, S165–S174.
- Slob, E., K. Wapenaar, F. Brogгинi, and R. Snieder, 2014, Seismic reflector imaging using internal multiples with Marchenko-type equations: *Geophysics*, **79**, S63–S76.
- Staring, M., R. Pereira, H. Douma, J. van der Neut, and K. Wapenaar, 2017, Adaptive double-focusing method for source-receiver Marchenko redatuming on field data: 87th Annual International Meeting, SEG, Expanded Abstracts, 4808–4812.
- Van der Neut, J., J. L. Johnson, K. van Wijk, S. Singh, E. Slob, and K. Wapenaar, 2017, A Marchenko equation for acoustic inverse source problems: *Journal of the Acoustical Society of America*, **141**, 4332–4346.
- Wapenaar, K., J. Brackenhoff, J. Thorbecke, J. van der Neut, E. Slob, and E. Verschuur, 2018, Virtual acoustics in inhomogeneous media with single-sided access: *Scientific Reports*, **8**, 2497.
- Wapenaar, K., F. Brogгинi, E. Slob, and R. Snieder, 2013, Three-dimensional single-sided Marchenko inverse scattering, data-driven focusing, Green's function retrieval, and their mutual relations: *Physical Review Letters*, **110**, 084301.
- Wapenaar, K., J. Thorbecke, and J. van der Neut, 2016, A single-sided homogeneous Green's function representation for holographic imaging, inverse scattering, time-reversal acoustics and interferometric Green's function retrieval: *Geophysical Journal International*, **205**, 531–535.
- Wapenaar, K., J. Thorbecke, J. van der Neut, F. Brogгинi, E. Slob, and R. Snieder, 2014, Marchenko imaging: *Geophysics*, **79**, WA39–WA57.
- Wapenaar, K., J. Thorbecke, J. van der Neut, E. Slob, and R. Snieder, 2017, Review paper: Virtual sources and their responses, Part II: data-driven single-sided focusing: *Geophysical Prospecting*, **65**, 1430–1451.